ChemComm

COMMUNICATION

View Article Online
View Journal | View Issue

Cite this: *Chem. Commun.*, 2018, **54**, 9155

Received 10th June 2018,
Accepted 20th July 2018

DOI: 10.1039/c8cc04621b

rsc.li/chemcomm

A core–shell nanoparticle–peptide@metal–organic framework as pH and enzyme dual-recognition switch for stepwise-responsive imaging in living cells†

Hong Shen, Jintong Liu, Jianping Lei * and Huangxian Ju

A core–shell nanostructure is fabricated with a pH-sensitive metal–organic framework shell and a peptide functionalized gold nanoparticle core *via* a mild synthetic route. The nanostructure can be applied as a dual-recognition switch in response to an acidic environment and enzyme activity, sequentially, leading to a stepwise-responsive strategy for imaging lysosomal cathepsin B.

Metal–organic frameworks (MOFs), a new class of crystalline molecular materials, are constructed by linking metal ions or clusters with organic bridging ligands in a well-defined coordination geometry.[1] In particular, nanoparticle functionalized MOF (NP@MOF) composites have attracted increasing attention due to their flexible properties and versatile functionalities.[2] Combining the benefits of both the nanoparticles and MOFs effectively, NP@MOFs have exhibited various application potentials in catalysis,[3] sensing,[4] drug delivery,[5] and biomedical applications.[6] For example, an electrochemical sensor based on electrocatalysis was constructed by one-pot encapsulation of platinum nanoparticles into a prototypal MOF for the detection of telomerase activity.[7] However, to date, little has been reported on developing a NP@MOF nanostructure as a recognition switch for biosensing and intracellular imaging. In this work, by taking advantages of NPs as a template and a recognition element, a core–shell NP@MOF system is designed as a dual-recognition switch for pH and enzymes *via* a stepwise-responsive strategy to monitor intracellular enzyme activity.

Cathepsin B (CaB) is one of the cysteine endopeptidases and is abundantly found in the lysosome, which plays key roles in the regulation of cellular metabolism.[8] The detection of enzyme activity and *in situ* imaging have made tremendous progresses using enzyme-responsive probes.[9] For example, a CaB-sensitive nanoprobe was developed by conjugating a self-quenched fluorogenic peptide onto the surface of tumor-targeting glycol chitosan nanoparticles for non-invasive optical imaging.[10] Furthermore, a lysosome-targeting fluorogenic small molecule probe was reported by incorporating morpholine into an aminoluciferin scaffold for fluorescence imaging of lysosomal CaB in living cells.[11] To further improve the probe's performance, it is necessary to deliver the recognition element to the specific site without exposure on the way. Considering the low pH conditions of CaB in the lysosome, it is beneficial to seek a facile and dual-triggered nanoplatform with acidic response for localized imaging of lysosomal CaB.

Zeolitic imidazolate framework-8 (ZIF-8) is becoming a promising delivery platform in biomedical application for its pH-sensitive and biocompatible properties.[12] By taking advantages of nanoparticles and MOFs, a core–shell NP@MOF nanoprobe named Au-Cy3P@ZIF-8 was fabricated by using pH-sensitive ZIF-8 as a shell and a cyanine 3 (Cy3)-labelled substrate peptide (Cy3-GRRGKC) (Fig. S1, ESI†) functionalized gold nanoparticle (Au-Cy3P) as a core in response to the acidic microenvironment and CaB activity, respectively (Scheme 1). The ZIF-8 shell of the nanoprobes could be disassembled under the acidic environment, and then the exposed substrate peptide with a cleavage site between arginine and glycine was recognized by CaB.[10] The fluorescence of the Cy3-labeled peptides on the gold nanoparticle (AuNP) core was turned on *via* the cleavage of CaB due to the departure of a Cy3-labeled fragment from the AuNP surface. Thus, a "signal on" strategy was established for CaB detection with high specificity and sensitivity. Upon cellular internalization, the imaging strategy could specifically distinguish lysosomal CaB, since the lysosome microenvironment (pH 4.5–6.0) is more acidic than the cytoplasm, resulting in a precisely localized imaging strategy for enzyme activity in living cells.

Au-Cy3P was synthesized by conjugating a Cy3-labeled peptide on the surface of the AuNPs *via* covalent binding of the Au–S bond. Then Au-Cy3P@ZIF-8 was prepared by encapsulating the Au-Cy3P core into ZIF-8 shells through a mild synthetic route, which could retain the biological activity of the substrate peptide for subsequent recognition toward CaB. From the scanning electron microscopy (SEM) images of the Au-Cy3P@ZIF-8 nanostructure (Fig. 1A)

State Key Laboratory of Analytical Chemistry for Life Science, School of Chemistry and Chemical Engineering, Nanjing University, Nanjing 210023, China.
E-mail: jpl@nju.edu.cn

† Electronic supplementary information (ESI) available: Materials, methods, characterization and supplementary data. See DOI: 10.1039/c8cc04621b

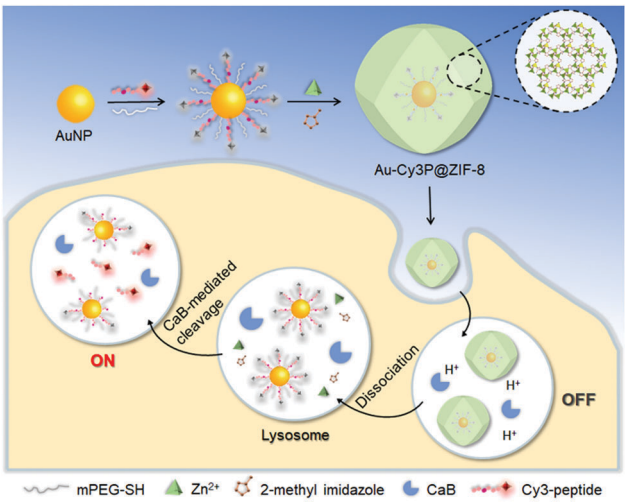

Scheme 1 Schematic illustration of the synthesis of a core–shell Au-Cy3P@ZIF-8 nanostructure and its application in a stepwise-responsive imaging strategy.

and pure ZIF-8 (Fig. S2, ESI†), monodispersed particles were observed in the form of spherical-like and faceted particles, indicating the initial stages of ZIF-8 crystallization.[13] The obtained Au-Cy3P had a uniform size of ~13 nm observed from the transmission electron microscopy (TEM) image (Fig. S3, ESI†), while Au-Cy3P@ZIF-8 displayed an average diameter of ~85 nm with a typical core–shell nanostructure from the TEM image (inset in Fig. 1A and Fig. S4, ESI†), demonstrating that the nanostructure was assembled by the encapsulation of an Au-Cy3P core into a ZIF-8 shell. The powder X-ray diffraction pattern (PXRD) of Au-Cy3P@ZIF-8 was similar to the peaks assigned to the pure ZIF-8 crystal structure (Fig. 1B), which validated the structure of ZIF-8 as shells and the maintenance of its intrinsic crystalline structure of ZIF-8.

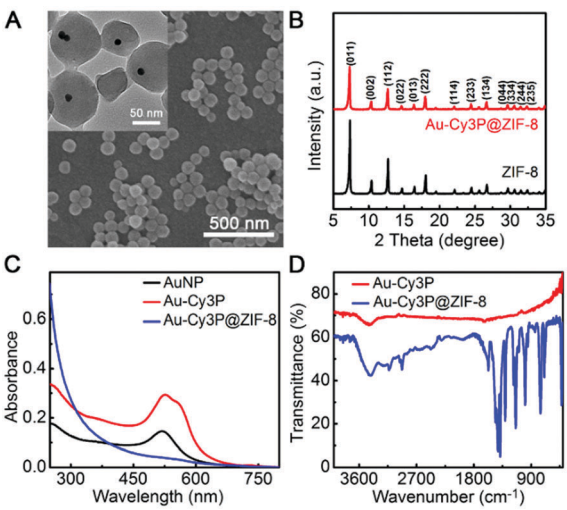

Fig. 1 (A) SEM image of Au-Cy3P@ZIF-8. Inset: TEM image of Au-Cy3P@ZIF-8. (B) PXRD patterns of pure ZIF-8 and Au-Cy3P@ZIF-8. (C) UV-vis absorption spectra of AuNPs, Au-Cy3P and Au-Cy3P@ZIF-8 in aqueous solution. (D) IR spectra of Au-Cy3P and Au-Cy3P@ZIF-8.

Furthermore, as shown in Fig. S5, ESI,† the mean hydrodynamic diameters of AuNPs, Au-Cy3P and Au-Cy3P@ZIF-8 were 14, 17 and 87 nm, respectively. The final diameter endowed Au-Cy3P@ZIF-8 with its potential use in cellular uptake by mammalian cells. In UV-vis spectra (Fig. 1C), Au-Cy3P showed a slight red-shift of the maximum peak from 521 nm to 527 nm, which manifested the successful loading of the Cy3-peptide on the AuNP surface. After the encapsulation into the ZIF-8 shells, the characteristic absorption of AuNPs became low since the scattering effect of the ZIF-8 shell weakened the intensity of the plasmon band,[14] suggesting the generation of the ZIF-8 shell. As shown in Fig. S6 (ESI†), the zeta potential of the as-prepared Au-Cy3P@ZIF-8 was +18.4 mV, in contrast to the negative state on the pure AuNPs (−11.8 mV) and Au-Cy3P (−2.9 mV), implying the layer-by-layer assembly. Moreover, Au-Cy3P@ZIF-8 displayed the characteristic bands of 2-MIm, such as the C–H stretching vibrational modes of the imidazole ring (3126 cm^{-1}), methyl group (2925 cm^{-1}), C=N stretching modes (1569 cm^{-1}), and the entire ring stretching (1326–1540 cm^{-1}) in the IR spectra (Fig. 1D). These analyses indicated the formation of core–shell nanostructures, which was consistent with the anticipated design.

In order to investigate the feasibility of the Au-Cy3P@ZIF-8 nanoprobe in response to intracellular lysosomal CaB, enzymatic assays *in vitro* were performed *via* contrastive experiments. To simulate the different pH environments of the lysosome and cytoplasm, pH 4.5 and pH 7.4 PBS buffers were chosen as the assay solutions. Fig. 2A illustrates the change of fluorescence intensity in response to CaB under different pH conditions. In the absence of CaB, no obvious fluorescence increase was observed although the nanoprobe was incubated in pH 4.5 buffer, revealing that the dissociation of the acid-sensitive shell alone could not bring about fluorescence recovery. In the presence of CaB, the fluorescence intensity of the nanoprobe in pH 4.5 buffer remarkably increased compared to that in pH 7.4 buffer, indicating that the CaB-responsive core was activated once the ZIF-8 shell was dissociated under the acidic environment. The increased fluorescence intensity could be attributed to the fluorescence recovery of the released Cy3 *via* CaB cleavage of the substrate peptide. In addition, the PXRD patterns (Fig. S7, ESI†) and the SEM images (Fig. S8, ESI†) of Au-Cy3P@ZIF-8 revealed the degradation of the ZIF-8 shell along with the incubation time in pH 4.5 buffer.

To further verify that the pH-sensitive properties were attributed to the ZIF-8 shell rather than the dye of Cy3, the fluorescence change was investigated in a series of different pH solutions. As shown in Fig. 2B, the fluorescence intensity of the Au-Cy3P@ZIF-8 nanoprobe increased gradually with the reduction of pH value and an obvious enhancement of fluorescence intensity was observed between pH 3.5 and 5.5, indicating the acidic-sensitive properties of the ZIF-8 shells. As a typical zeolitic imidazolate framework, ZIF-8 is coordinated by zinc and imidazolate ions, and its coordination bonds are hydrolyzed at pH 5.0–6.0.[15] Depending on the pH, the decomposition of ZIF-8 increased intensively with the enhancement of the environmental acidity. When the pH value was lower than 4.5, the fluorescence intensity of the nanoprobe no longer enhanced significantly. Therefore we chose 4.5 as the optimal pH, which was close to

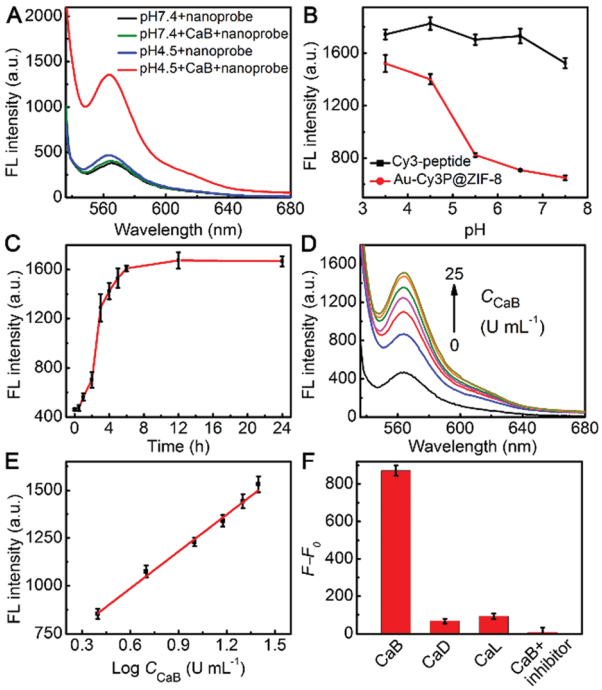

Fig. 2 (A) Fluorescence spectra of 50 μg mL^{-1} Au-Cy3P@ZIF-8 nanoprobe incubated in pH 7.4 and 4.5 PBS (10 mM) in the presence and absence of 15 U mL^{-1} CaB for 6 h. (B) Dependence of fluorescence intensities of Au-Cy3P@ZIF-8 nanoprobe and Cy3-peptide on pH. (C) Plot of fluorescence intensity of Au-Cy3P@ZIF-8 nanoprobe after incubation for 0, 0.5, 1, 2, 3, 4, 5, 6, 12 and 24 h in pH 4.5 PBS containing 15 U mL^{-1} CaB. (D) Fluorescence spectra of Au-Cy3P@ZIF-8 nanoprobe after incubation with 0, 2.5, 5, 10, 15, 20 and 25 U mL^{-1} CaB (from bottom to top) for 6 h in pH 4.5 PBS. (E) Plot of fluorescence intensity *vs.* the logarithm value of CaB concentration. (F) Difference of fluorescence intensity of Au-Cy3P@ZIF-8 nanoprobe at 514 nm before (F_0) and after (F) treatment with 15 U mL^{-1} CaB, CaD, CaL, and a mixture of CaB and its inhibitor for 6 h in pH 4.5 PBS.

the pH value in lysosomes and available for intracellular experiments considering the lysosomal microenvironment. In addition, the fluorescence intensity of Cy3-labeled peptides remained unchanged in the pH range of 3.5–7.5, indicating that the dye of Cy3 had negligible dependency on the pH, which eliminated the interference of the fluorescence intensity change caused by the pH-dependent properties of the dye.

At the optimal pH of 4.5, the Au-Cy3P@ZIF-8 nanoprobe was incubated for different times. The fluorescence intensity of the probe increased gradually with time, indicating the time-dependent dissociation of ZIF-8 shells. After 6 h, the fluorescence intensity of the nanoprobe reached a plateau, demonstrating that the optimized incubation time is 6 h (Fig. 2C). Under the optimum conditions, fluorescence intensities of the nanoprobe (50 μg mL^{-1}) were measured at 514 nm in CaB solution with varying concentrations (Fig. 2D). It was clear to see that the increase of CaB concentration led to enhancements in fluorescence intensity, indicating a CaB concentration-dependent cleavage of the nanoprobe. The fluorescence intensity at 514 nm was linearly proportional to the logarithm value of concentration of CaB from 2.5 to 25 U mL^{-1} (Fig. 2E), which is feasible to monitor the CaB activity in the lysosome of cancer cells.[16]

Next, the specificity for CaB was investigated upon incubation with CaB and its relative cathepsins by comparing the change in fluorescence intensity. As shown in Fig. 2F, the difference in fluorescence intensity for the nanoprobe treated with CaB was approximately 9.4- and 12.9-fold higher than those treated with CaL and CaD, respectively. Furthermore, the noticeable enhancement in fluorescence intensity at 514 nm was entirely restrained by the CaB inhibitor. These results suggested a good selectivity of the nanoprobe towards CaB by eliminating the interference from cross-reactivity of other cathepsins.

To confirm the possibility of the Au-Cy3P@ZIF-8 nanoprobe for imaging of intracellular CaB activities, we first evaluated its cytotoxicity against HeLa cancer cells using the CCK-8 assay. Upon incubation with a fixed concentration of the nanoprobe (50 μg mL^{-1}) for different times and with varying concentrations of the nanoprobe for 8 h (Fig. S9, ESI†), no adverse effect on cell viability was observed, demonstrating a high biocompatibility of the Au-Cy3P@ZIF-8 nanoprobes to living cells.

To further certify the location of CaB activity in the lysosome, colocalization experiments were performed with the lysosomal tracker Green DND-26 which could specifically mark the lysosomes of the cells. As shown in Fig. 3, HeLa cells incubated with the Au-Cy3P@ZIF-8 nanoprobe showed bright red fluorescence spots, which overlapped very well with the green fluorescence emitted from the intracellular lysosomal tracker. This phenomenon could be explained by the fact that the nanoprobes were effectively taken up by the HeLa cells and entrapped into the lysosome where the CaB-responsive cores were unlocked from the ZIF-8 shell and the fluorescence of Cy3 was turned on by the lysosomal CaB. These results indicated that the Au-Cy3P@ZIF-8 nanoprobe has the capacity for precisely localized probing the CaB activity.

The optimized incubation conditions of the Au-Cy3P@ZIF-8 nanoprobe such as the culturing time and concentration were investigated. After 4 h incubation of HeLa cells with the nanoprobe, some fluorescent spots of Cy3 were observed in the cells (Fig. S10, ESI†), indicating the dissociation of ZIF-8 shells and subsequent activation of the CaB-responsive cores of the uptaken nanoprobe. The amount and fluorescence intensity of

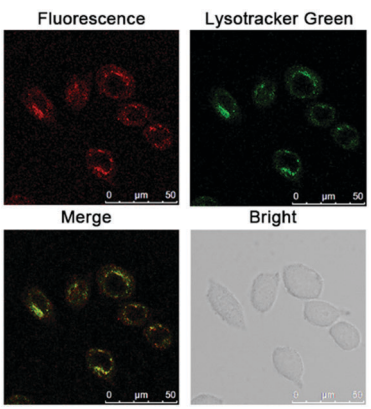

Fig. 3 Colocalization images of 50 μg mL^{-1} Au-Cy3P@ZIF-8 nanoprobes with LysoTracker Green in HeLa cells. Scale bar: 50 μm.

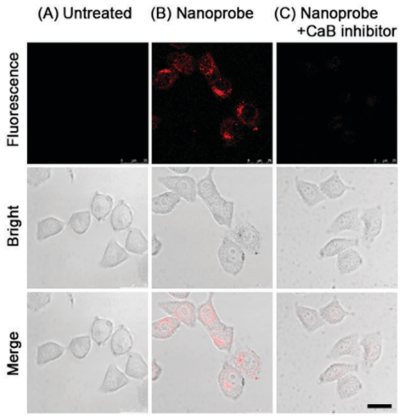

Fig. 4 Confocal fluorescence images of HeLa cells: (A) untreated, (B) treated with 50 μg mL^{-1} Au-Cy3P@ZIF-8 nanoprobe and (C) 50 μg mL^{-1} Au-Cy3P@ZIF-8 nanoprobe + 10 ng mL^{-1} CaB inhibitor at 37 °C for 8 h. Scale bar: 25 μm.

the fluorescent spots increased gradually with increasing incubation time and reached a plateau at 8 h. In addition, a similar concentration-dependent fluorescence enhancement was observed in the concentration of the nanoprobe ranging from 5 μg mL^{-1} to 50 μg mL^{-1} (Fig. S11, ESI†). Therefore, we selected the concentration of 50 μg mL^{-1} and the incubation time of 8 h as the optimum conditions for the following fluorescence imaging of lysosomal CaB.

HeLa cells when treated with the Au-Cy3P@ZIF-8 nanoprobe (50 μg mL^{-1}) for 8 h exhibited much enhanced fluorescence than the cells without treatment (Fig. 4), indicating that the nanoprobes were effectively taken up by the cells and entrapped into the lysosomes for CaB-activated fluorescence turn-on. The intensive fluorescence was distributed in the lysosome, which is consistent with the result of colocalization experiments for localized imaging. Moreover, the CaB inhibitor-treated cells displayed no obvious fluorescence, suggesting that the fluorescence recovery was specifically triggered by the intracellular CaB. Therefore, the Au-Cy3P@ZIF-8 nanoprobe as a dual-recognition switch successfully realized the more accurate fluorescence imaging of lysosomal CaB in living cells.

In summary, we have successfully developed a core–shell NP@MOF nanostructure as a dual-recognition switch for monitoring lysosomal CaB activity *via* a stepwise-responsive localized imaging strategy. To the best of our knowledge, it is the first time that a bio-recognition switch is embedded into a MOF for accurate imaging of localized enzyme activity. As an efficient degradable system, the ZIF-8 shell with nontoxicity and good biocompatibility is beneficial for retaining the biological activity of the substrate peptide, and has a highly activated response to the acidic environment. Sequentially, the exposed Au–peptide core of the nanoprobes was recognized by CaB, realizing a stepwise-responsive strategy for CaB detection with high specificity and sensitivity. After delivery into HeLa cells, the fluorescence of the nanoprobe could be turned on effectively owing to the pH and CaB dual-responsive properties of NP@MOF in the lysosome. Intracellular colocalization imaging results further verified the capability of the nanoprobe for localized fluorescence imaging. The current work not only sheds new insights into the design and fabrication of highly efficient dual-recognition nanoplatforms, but also demonstrates a concept of stepwise-responsive imaging approach for accurate biomedical applications.

We gratefully acknowledge the National Natural Science Foundation of China (21675084 and 21635005) and the National Key Technologies R&D Program (2016YFC0302500).

Conflicts of interest

There are no conflicts to declare.

Notes and references

1 (*a*) B. Li, H. M. Wen, Y. J. Cui, W. Zhou, G. D. Qian and B. L. Chen, *Adv. Mater.*, 2016, **28**, 8819; (*b*) M. Nazari, M. Rubio-Martinez, G. Tobias, J. P. Barrio, R. Babarao, F. Nazari, K. Konstas, B. W. Muir, S. F. Collins, A. J. Hill, M. C. Duke and M. R. Hill, *Adv. Funct. Mater.*, 2016, **26**, 3244; (*c*) X. Z. Lian, Y. Fang, E. Joseph, Q. Wang, J. L. Li, S. Banerjee, C. Lollar, X. Wang and H. C. Zhou, *Chem. Soc. Rev.*, 2017, **46**, 3386; (*d*) W. H. Chen, X. Yu, W. C. Liao, Y. S. Sohn, A. Cecconello, A. Kozell, R. Nechushtai and I. Willner, *Adv. Funct. Mater.*, 2017, 1702102.
2 (*a*) G. Lu, S. Z. Li, Z. Guo, O. K. Farha, B. G. Hauser, X. Y. Qi, Y. Wang, X. Wang, S. Y. Han, X. G. Liu, J. S. DuChene, H. Zhang, Q. C. Zhang, X. D. Chen, J. Ma, S. C. Joachim Loo, W. D. Wei, Y. H. Yang, J. T. Hupp and F. W. Huo, *Nat. Chem.*, 2012, **4**, 310; (*b*) J. J. Zhou, P. Wang, C. X. Wang, Y. T. Goh, Z. Fang, P. B. Messersmith and H. W. Duan, *ACS Nano*, 2015, **9**, 6951; (*c*) Y. L. Liu and Z. Y. Tang, *Adv. Mater.*, 2013, **25**, 5819.
3 (*a*) P. Li and H. C. Zeng, *Chem. Commun.*, 2017, **53**, 6025; (*b*) S. L. Zhang, A. J. Han, Y. L. Zhai, J. Zhang, W. C. Cheong, D. S. Wang and Y. D. Li, *Chem. Commun.*, 2017, **53**, 9490.
4 (*a*) H. S. Wang, H. L. Liu, K. Wang, Y. Ding, J. J. Xu, X. H. Xia and H. Y. Chen, *Anal. Chem.*, 2017, **89**, 11366; (*b*) J. Li, J. X. Wang, Y. Ling, Z. X. Chen, M. X. Gao, X. M. Zhang and Y. M. Zhou, *Chem. Commun.*, 2017, **53**, 4018.
5 M. X. Wu and Y. W. Yang, *Adv. Mater.*, 2017, 1606134.
6 (*a*) W. Q. Wang, L. Wang, Y. Li, S. Liu, Z. G. Xie and X. B. Jing, *Adv. Mater.*, 2016, **28**, 9320; (*b*) X. H. Zheng, L. Wang, Q. Pei, S. S. He, S. Liu and Z. G. Xie, *Chem. Mater.*, 2017, **29**, 2374.
7 P. H. Ling, J. P. Lei, L. Jia and H. X. Ju, *Chem. Commun.*, 2016, **52**, 1226.
8 (*a*) P. K. Tsung, J. B. Lombardini and F. J. Holly, *Exp. Eye Res.*, 1984, **38**, 73; (*b*) S. Y. Yan and B. F. Sloane, *Biol. Chem.*, 2003, **384**, 845; (*c*) G. Mikhaylov, D. Klimpel, N. Schaschke, U. Mikac, M. Vizovisek, M. Fonovic, V. Turk, B. Turk and O. Vasiljeva, *Angew. Chem., Int. Ed.*, 2014, **53**, 10077.
9 (*a*) Z. H. Zeng, S. Mizukami, K. Fujita and K. Kikuchi, *Chem. Sci.*, 2015, **6**, 4934; (*b*) A. A. Beharry, S. Lacoste, T. R. O'Connor and E. T. Kool, *J. Am. Chem. Soc.*, 2016, **138**, 3647; (*c*) J. X. Aw, F. Widjaja, Y. C. Ding, J. Mu, Y. Liang and B. G. Xing, *Chem. Commun.*, 2017, **53**, 3330; (*d*) M. M. He, Z. Han, J. Qiao, L. Ngo, M. P. Xiong and Y. G. Zheng, *Chem. Commun.*, 2018, **54**, 5594.
10 J. H. Ryu, J. H. Na, H. K. Ko, D. G. You, S. Park, E. Jun, H. J. Yeom, D. H. Seo, J. H. Park, S. Y. Jeong, I. S. Kim, B. S. Kim, I. C. Kwon, K. Choi and K. Kim, *Biomaterials*, 2014, **35**, 2302.
11 Y. Q. Wang, J. B. Li, L. D. Feng, J. F. Yu, Y. Zhang, D. J. Ye and H. Y. Chen, *Anal. Chem.*, 2016, **88**, 12403.
12 (*a*) R. Chen, J. F. Zhang, Y. Wang, X. F. Chen, J. A. Zapien and C. S. Lee, *Nanoscale*, 2015, **7**, 17299; (*b*) Z. F. Wang, X. J. Tang, X. X. Wang, D. D. Yang, C. Yang, Y. B. Lou, J. X. Chen and N. Y. He, *Chem. Commun.*, 2016, **52**, 12210; (*c*) Y. Duan, F. G. Ye, Y. L. Huang, Y. M. Qin, C. M. He and S. L. Zhao, *Chem. Commun.*, 2018, **54**, 5377.
13 S. R. Venna, J. B. Jasinski and M. A. Carreon, *J. Am. Chem. Soc.*, 2010, **132**, 18030.
14 L. M. Liz-Marzán, M. Giersig and P. Mulvaney, *Langmuir*, 1996, **12**, 4329.
15 J. Zhuang, C. H. Kuo, L. Y. Chou, D. Y. Liu, E. Weerapana and C. K. Tsung, *ACS Nano*, 2014, **8**, 2812.
16 B. Ulbricht, E. Spiess, R. Schwartz-Albiez and W. Ebert, *Biol. Chem. Hoppe-Seyler*, 1995, **376**, 407.

